Agricultural and Forest Meteorology 256–257 (2018) 150–158

Contents lists available at ScienceDirect

Agricultural and Forest Meteorology

journal homepage: www.elsevier.com/locate/agrformet

# Global patterns of vegetation carbon use efficiency and their climate drivers deduced from MODIS satellite data and process-based models

Yue He[a], Shilong Piao[a,*], Xiangyi Li[a], Anping Chen[b], Dahe Qin[c,d]

[a] Sino-French Institute for Earth System Science, College of Urban and Environmental Sciences, Peking University, Beijing 100871, China
[b] Department of Forestry and Natural Resources, Purdue University, West Lafayette, IN 46907, USA
[c] State Key Laboratory of Cryospheric Sciences, Northwest Institute of Eco-environment and Resources, Chinese Academy of Sciences, Lanzhou 730000, China
[d] National Climate Center, China Meteorological Administration, Beijing 100081, China

ARTICLE INFO

*Keywords:*
Autotrophic respiration ($R_a$)
Carbon cycle models
Carbon use efficiency (CUE)
Climate change
Gross primary production (GPP)
MODIS

ABSTRACT

Carbon use efficiency (CUE), defined as the ratio of net primary production (NPP) to gross primary production (GPP), represents the capacity of plants in converting assimilated atmospheric carbon dioxide to ecosystem carbon storage. Process-based models are important tools for simulating NPP and GPP; yet the model performance in simulating vegetation CUE has not been fully explored. The goal of this paper is thus to investigate the spatial variations in CUE from different process-based carbon cycle models in comparison with that from Moderate Resolution Imaging Spectroradiometer (MODIS) satellite data, and to analyze their linkage with climate factors. The global average CUE derived from the five process-based models is 0.45 ± 0.05 (range from 0.38 to 0.52), slightly lower than the value of 0.48 obtained from MODIS data. A strong latitudinal gradient of CUE, with greater CUE at high latitudes, is well agreed by these different datasets. However, there also exist considerable discrepancies in CUE estimations among those products, especially in temperate Northern Hemisphere. Furthermore, for both the satellite-based dataset and results from process-based models, vegetation CUE declines non-linearly with increase in temperature, but remains relatively stable with enhanced precipitation. Our results also indicate that the differences in global patterns of CUE estimated by different approaches could be primarily resulted from their systematic differences in autotrophic respiration ($R_a$) rather than in GPP. Understanding mechanisms behind spatio-temporal changes in $R_a$ is therefore a critical step towards better quantifying global CUE.

## 1. Introduction

Carbon use efficiency (CUE), which is defined as the proportion of gross primary production (GPP, $g\,C\,m^{-2}\,yr^{-1}$) converted into net primary production (NPP, $g\,C\,m^{-2}\,yr^{-1}$), represents the efficiency of plants to sequester carbon from the atmosphere and is increasingly recognized as an important parameter shaping ecosystem carbon storage (Gifford, 2003; Chambers et al., 2004; De Lucia et al., 2007; Zhang et al., 2009; Piao et al., 2010; Vicca et al., 2012; Bradford & Crowther, 2013; Campioli et al., 2015). In practice, GPP usually represents the total amount of carbon captured through photosynthesis, and NPP is the net carbon stored in plant as new material after the reduction of GPP through autotrophic respiration ($R_a$, $g\,C\,m^{-2}\,yr^{-1}$) (Chapin et al., 2002). Therefore, this dimensionless parameter is also a measure of how GPP is partitioned into NPP and $R_a$, which could have a deep impact on vegetation structure and functioning (Ise et al., 2010). In particular, quantifying the responses of vegetation CUE to its climatic drivers could improve our understanding of the dynamics of biosphere-atmosphere carbon exchange under current and future climate change (Ise et al., 2010; Bloom et al., 2016).

Earlier terrestrial carbon-cycle models like CASA (Potter et al., 1993) and FOREST-BGC (Running & Coughlan, 1988) often assumed a fixed value of CUE to quantify $R_a$ (De Lucia et al., 2007). However, there is increasing evidence suggesting that CUE actually varies with many factors, including vegetation type, climate conditions, management status, site fertility and forest stand age (Ryan et al., 1997; Amthor, 2000; Mäkelä & Valentine, 2001; Giardina et al., 2003; De Lucia et al., 2007; Piao et al., 2010; Vicca et al., 2012; Campioli et al., 2015). As an example, forest ecosystem CUE, according to a meta-analysis of 60 observations, ranged from 0.23 to 0.83 among different forest types (De Lucia et al., 2007).

The spatial variation of vegetation CUE across the global land and its association with environmental factors, however, remain poorly understood; although there have been many measurements of

* Corresponding author.
*E-mail address:* slpiao@pku.edu.cn (S. Piao).

https://doi.org/10.1016/j.agrformet.2018.03.009
Received 29 September 2017; Received in revised form 8 March 2018; Accepted 12 March 2018
Available online 20 March 2018
0168-1923/ © 2018 Elsevier B.V. All rights reserved.

vegetation CUE at stand or site level (Ryan et al., 1997; Giardina et al., 2003; Van Iersel, 2003; Law et al., 2004; Metcalfe et al., 2010). The challenge comes from both the lack of sufficient observations and the large uncertainty generated in direct up-scaling from site measurements to larger spatial scale estimates. Recently, Zhang et al. (2009) used GPP and NPP products derived from the Moderate Resolution Imaging Spectroradiometer (MODIS) to estimate the global distribution of vegetation CUE. Yet, the conclusion drawn from a single dataset is sensitive to its systematic biases and errors, making it critical to compare global patterns of vegetation CUE among different datasets. On the other hand, newly-emerged process-based carbon cycle models have been widely used to simulate major physiological and ecological processes (e.g., photosynthesis, respiration, carbon allocation and phenology) and ecosystem structures (Moorcroft, 2006; Huntingford et al., 2011; Wang et al., 2014a,b; Prentice et al., 2015; Wang et al., 2016; Piao et al., 2017; Liu et al., 2018; Wu et al., 2018). These process-based models may provide us a new approach to estimate vegetation CUE at the global scale.

Currently there are a variety of approaches available in obtaining CUE at the global scale (Ise et al., 2010; Zhang et al., 2009, 2014). But none of them are solely based on observations but rely upon certain assumptions and simplifications about model structures and parameters in simulating photosynthesis and autotrophic respiration. Hence, there is no consensus on the spatial variation of vegetation CUE and its drivers among different data streams. It is necessary to identify the sources of variation in CUE simulated by different models and/or dataset (MODIS), which could inform us of the potential uncertainties in the simulation of CUE and provide guidance on the future model development.

Here we conducted a systematic study of spatial patterns of vegetation CUE and their climatic drivers based upon MODIS satellite data and five process-based models. Moreover, we also examined the discrepancies in modelled CUE among different datasets and explored the potential reasons.

## 2. Material and methods

### 2.1. MODIS satellite data

Similar to the studies of Zhang et al. (2009; 2014), we used the MODIS GPP and NPP products (collection-055) over the period 2000–2012 (downloaded from http://files.ntsg.umt.edu/data/NTSG_Products/MOD17/GeoTIFF/MOD17A3/GeoTIFF_30arcsec/) to calculate vegetation CUE. The MODIS algorithm integrates a light use efficiency logic using satellite observed LAI/FPAR to estimate GPP with an autotrophic respiration module to derive NPP (Running et al., 2004; Zhao et al., 2006; Zhao & Running, 2010). Both GPP and NPP in MODIS are driven by the NCEP/DOE II reanalysis climatic dataset (http://www.esrl.noaa.gov). In addition to using satellite and climate data as inputs, it also requires biophysical parameters of biomes that are stored in the biome parameter look-up table (BPLUT). The uncertainties in the MODIS algorithm and its input data could lead to the biased estimation of NPP and GPP compared to in-situ measurements (e.g. Zhang et al., 2009, 2014; Sjöström et al., 2013). Note that the latest collection-6 MODIS NPP/GPP products (ftp://ladsweb.nascom.nasa.gov/allData/6/) were not used in our study because of large data gaps in this version. For example, in MODIS NPP product, there are some missing tiles in western Africa, most of Europe and the regions north of 60 °N (Fig. A.1 in Supplementary materials). We found that the estimated MODIS CUE from the collection-6 show higher values in the temperate zone of the two hemispheres and lower values in African sub-Sahel areas than those from collection-55 over the common region and periods (Fig. A.1 in Supplementary materials), suggesting the uncertainty of MODIS product in characterizing productivity. We therefore do not contend that MODIS CUE is necessarily more accurate than any of the five process model simulations.

### 2.2. Process-based carbon cycle models

This study used global annual GPP and NPP simulated by five process-based carbon cycle models: the CSIRO Atmosphere Biosphere Land Exchange-3.5 (CABLE) (Wang et al., 2010, 2011); Community Land Model-4.0 (CLM4CN) (Thornton et al., 2007); Lund-Potsdam-Jena (LPJ) (Sitch et al., 2003); Organizing Carbon and Hydrology in Dynamic Ecosystems (ORCHIDEE) (Krinner et al., 2005); and Vegetation Integrative Simulator for Trace gases (VISIT) (Ito, 2010). All these models were run at a spatial resolution of 0.5° (Huang et al., 2015; Piao et al., 2015). Here, we focus on the model simulations which were driven by observed climate change based on CRU-NCEP v.4 (http://dods. extra.cea.fr /data/ p529viov/ cruncep/) and the observed increasing atmospheric $CO_2$ concentrations. Note that CLM4CN and CABLE have taken nitrogen cycle into account; therefore effects of nitrogen-limitation in photosynthesis could be assessed. Further information about the characteristics of each model is listed in Supplementary Table A.1, and the main processes and parameters of photosynthesis and autotrophic respiration in Supplementary Table A.2.

### 2.3. Analyses

Because MODIS satellite data start in 2000, we used the simulations of the five process-based models from 2000 to the latest year available (different datasets have different time series, see Table A.1 in Supplementary materials). GPP and NPP outputs from MODIS data were re-gridded to 0.5° spatial resolution to be consistent with those of the process-based model outputs. Then, the monthly outputs of GPP and NPP from process-based models were combined to give annual values. To rule out areas with negligible vegetation, those pixels with mean annual normalized difference vegetation index (NDVI) lower than 0.1 were excluded from the analysis (Piao et al., 2014; Zhu et al., 2016; Wang et al., 2017). The vegetation CUE at the pixel scale was calculated as:

$$CUE = \frac{NPP}{GPP} \tag{1}$$

where NPP refers to annual net primary productivity (g C $m^{-2}$ $yr^{-1}$) and GPP to annual gross primary productivity (g C $m^{-2}$ $yr^{-1}$). Then, the yearly CUE was further averaged across the full study period to obtain multi-year mean value at the pixel scale. On the other hand, we calculated the yearly global mean CUE based on the average of CUE from all pixels. In addition to the area, the CUE in each pixel is also weighted by its GPP, which ensures that the regions with higher productivity will contribute more to the global mean CUE.

To compare the spatial patterns of vegetation CUE in the MODIS data with that produced by the process-based models, we applied the comparison map profile (CMP) method — a statistic-based new way in comparing two spatially explicit datasets (Gaucherel et al., 2008). This method estimates similarity indices between the two datasets using moving windows to compare their relationships at multiple spatial scales simultaneously. Firstly, the absolute value of the distance (D) between the means of dataset $x$ and dataset $y$ is computed according to the equation:

$$D = |\bar{x} - \bar{y}| \tag{2}$$

where both $\bar{x}$ and $\bar{y}$ are sample means of their moving windows respectively. Secondly, another similarity is obtained by the cross-correlation coefficient (CC) to compare the spatial data structures:

$$CC = \frac{1}{N^2} \sum_{i=1}^{N} \sum_{j=1}^{N} \frac{(x_{ij} - \bar{x})(y_{ij} - \bar{y})}{\sigma_x \sigma_y} \tag{3}$$

with

$$\sigma_x^2 = \frac{1}{N^2 - 1} \sum_{i=1}^{N} \sum_{j=1}^{N} (x_{ij} - \bar{x})^2 \quad (4)$$

where $x_{ij}$ (or $y_{ij}$) is the value in the $i^{th}$row and $j^{th}$column of the moving window, which has N pixels. For each of the two similarity indices, re-computing the index 20 times by gradually increasing the size of moving windows from 3 × 3 to 41 × 41 pixels (representative of 1–20 mono-scales). After that, 20 similarity maps for each index could be obtained. The 1-3 mono scale similarity maps were then eliminated to avoid overestimation at very small window sizes (Gaucherel et al., 2008). We thus obtained a multi-scale distance map and a cross-correlation map between the two spatially explicit datasets though averaging the 4–20 mono scale similarity maps respectively. More detailed information of this CMP method can be referenced to Gaucherel et al. (2008).

Because vegetation CUE is mainly determined by the physiological processes of photosynthesis and autotrophic respiration, CUE can be also defined as Eq. (5). In order to detect the discrepancies between CUE from MODIS satellite data and CUE from process-based models, the percentage differences of $R_a$ between MODIS and the five process-based models were calculated as Eq. (6), and the percentage differences in GPP were computed in the same way.

$$CUE = 1 - \frac{R_a}{GPP} \quad (5)$$

$$\%\Delta Model\ R_a = \left( \frac{Model\ R_a – MODIS\ R_a}{MODIS\ R_a} \right) \times 100\% \quad (6)$$

We also detected the discrepancies of CUE among the five process-based models by examining their differences in GPP and $R_a$. Partial correlation analysis was used between the three components of Eq. (7) below in each pixel on a global scale, and the corresponding variable with larger partial correlation coefficient represents the dominant factor inducing the discrepancies among the five models.

$$\ln(1 - CUE) = \ln(R_a) - \ln(GPP) \quad (7)$$

To analyze the responses of vegetation CUE to mean annual temperature (MAT) and mean annual precipitation (MAP), we used the climate data derived from the Climatic Research Unit database (CRU TS 3.21, http://www.cru.uea.ac.uk/, Harris et al., 2014). Note that regions occupying a very small portion of the world with MAT higher than 30 °C (or lower than -20 °C) and regions with MAP over 4000 mm were ruled out from this analysis. Vegetation CUE from different datasets on a global scale was firstly binned into intervals of 0.1 °C MAT and 20 mm MAP, and area-weighted averages of CUE were calculated for each interval. We then drew up the relationship between CUE and MAT (MAP) under different MAP (MAT) bins. After that, the responses of CUE to MAT (or MAP) under adjacent bins with similar distributions were merged together. As a result, the relationship between CUE and MAP was divided into five temperature intervals: -20-0 °C, 0-10 °C, 10-15 °C, 15-20 °C and 20-30 °C. Likewise, the relationship between CUE and MAT was divided into five precipitation intervals: 0-400 mm, 400-600 mm, 600-1000 mm, 1000-1500 mm, and 1500-4000 mm. The changes of CUE with MAT (or MAP) were then smoothed by moving average over 1 °C (or 100 mm).

We further applied partial correlation analysis to determine the correlation of CUE with temperature, precipitation, and incoming shortwave radiation. The radiation data is derived from CRU-NCEP v6.1 (http://dods.extra.cea.fr/data/p529viov/cruncep/, Viovy, 2015). Spatial partial correlation coefficients were then calculated using a moving window of 5.5° × 5.5° surrounding each 0.5° grid cell.

Here we use Lindeman-Merenda-Gold (LMG; Lindeman et al., 1980) method to obtain the relative importance of the three climate factors (i.e., temperature, precipitation and radiation) in determining CUE variations. This analysis was conducted based on the package "relaimpo" (Grömping, 2006) in R software v3.4.3.

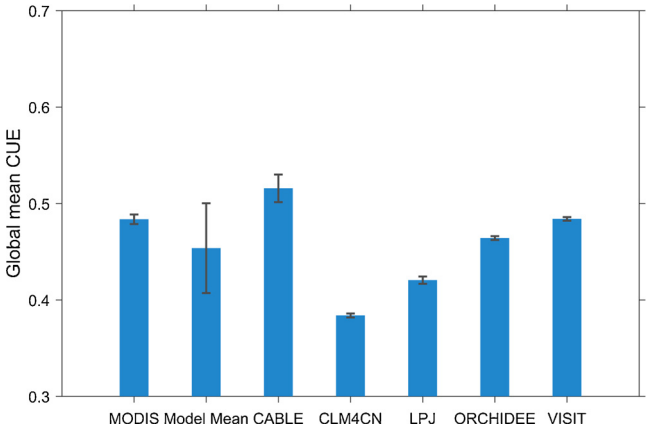


**Fig. 1.** Global mean carbon use efficiencies (CUE) from MODIS satellite data and five process-based models. Blue bars represent the global mean values of CUE estimated by satellite and model products. For global mean CUE of each product, the black error bars show the standard deviations over the study period. For the model mean global CUE, the black error bar represents the standard deviation of global CUE across different models.

## 3. Results

### 3.1. Global CUE

As shown in Fig. 1, the global mean CUE derived from process-based models is about 0.45 ± 0.05 (mean ± standard deviation), ranging from 0.38 ± 0.002 to 0.52 ± 0.010. This model derived CUE is slightly lower than the value obtained from the MODIS satellite data (0.48 ± 0.005). Among the models, global mean CUE is highest by CABLE (0.52 ± 0.010), followed by VISIT and ORCHIDEE, which have comparable values (0.48 ± 0.002 and 0.46 ± 0.002, respectively) similar to CUE derived from the MODIS data. The CUE estimates are smallest by the LPJ and CLM4CN models (0.42 ± 0.004 and 0.38 ± 0.002, respectively) (Fig. 1).

### 3.2. Spatial patterns of CUE

Fig. 2 shows the spatial distributions of vegetation CUE generated from the MODIS product and the five process-based models. All the datasets consistently show that boreal regions have higher CUE values than other regions, although there exist considerable differences in the magnitude of CUE estimates among different products. For example, the average CUE of boreal regions simulated by CABLE (0.65 ± 0.019) is 63% higher than that by CLM4CN (0.40 ± 0.002) (Table A.3 in Supplementary materials). Furthermore, while the products agree well on regions of the highest CUE values, they differ greatly on locations with the lowest ones. For example, according to the MODIS product, low CUE (< 0.2) values are generally found in arid regions, such as western Australia, African sub-Sahel savannas, and northern India (Fig. 2). However, the ORCHIDEE and LPJ models estimate lowest values (< 0.2) over western United States and central Asia. In contrast, the lowest CUE values estimated by CABLE are found in tropical rainforests including Amazonia and central Africa rainforests. For CLM4CN, the lowest CUE is found in northern European forests and Canadian forests.

We used the CMP method to quantitatively compare CUE generated from process-based models and from MODIS data. As stated previously, we used the MODIS product as a reference for modelled CUE comparisons, rather than assuming better data quality of the satellite-derived values over that from process-based models. The resulted mean CUE distance maps show that VISIT CUE is closest to MODIS CUE (global mean distance < 0.07), while LPJ and CLM4CN exhibit larger deviations from MODIS CUE (global mean distance > 0.18), especially in temperate Northern Hemisphere (Fig. 3a–e). In addition, process-based model estimated CUE is generally positively correlated with MODIS

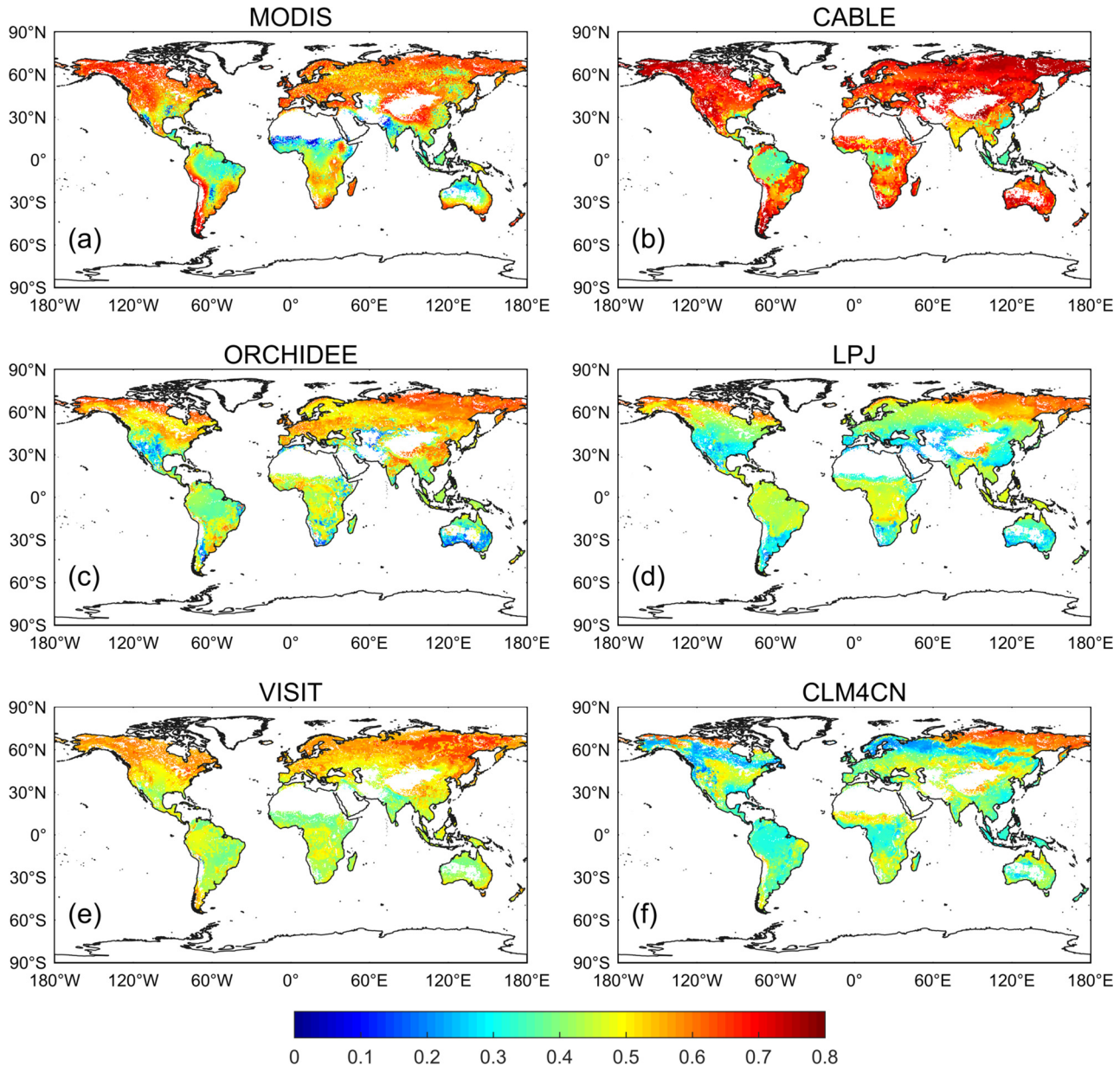


**Fig. 2.** Global patterns of vegetation carbon use efficiency (CUE) derived from (a) MODIS satellite data and (b)-(f) process-based models: CABLE, ORCHIDEE, LPJ, VISIT, and CLM4CN, averaged from 2000 to the latest year available.

CUE over most areas with similar mean correlation coefficients, despite of some occasional negative correlations in various regions (Fig. 3f–j). We also find a good agreement among modelled CUEs over the boreal region except for CABLE CUE, which is generally higher than other modelled values (Fig. A.2 in Supplementary materials). The largest discrepancies between MODIS and process-based model estimated CUE occur in temperate Northern and Southern Hemispheres (Fig. A.2 and Table A.2 in Supplementary materials).

In order to detect the differences in CUE estimates among the five process-based models, we then used the median absolute deviation (MAD) as a robust estimator (Fig. A.3 in Supplementary materials). Spatially, most of the largest discrepancies are found over temperate regions, especially in central Asia where the spread of CUE among different models is between 0.25 ± 0.003 from ORCHIDEE and 0.69 ± 0.012 from CABLE (Fig. 2). The smallest discrepancies are again found in boreal areas, where the MAD is close to zero.

### 3.3. Spatial variation of CUE in response to climate factors

As shown in Fig. 4a, MODIS CUE decreases non-linearly with increasing MAT, with CUE declining more rapidly after about 15-20 °C. In general, MODIS CUE under different precipitation bins shows similar variations in response to MAT (Fig. 4). Changes of CUE to MAT from most of the process-based models are broadly consistent with that of MODIS product, with higher CUE estimates in colder regions. However, CLM4CN fails to capture the decreasing CUE with increasing MAT when MAP is above ~1000 mm (Fig. 4e and f). Three process-based models (i.e., ORCHIDEE, LPJ and CLM4CN) show a distinct dip in the relationship between CUE and MAT at the MAT range between -10 °C and 20 °C, which is attributed to the possibility that these models simulate the lowest CUE values in temperate zones (Fig. 2).

Fig. 5 describes the changes of CUE in response to MAP variances for different MAT intervals. MODIS CUE first shows a decreasing trend with enhanced MAP, and then remains relatively stable when precipitation is above around 2100 mm (Fig. 5a). The results of the process-based

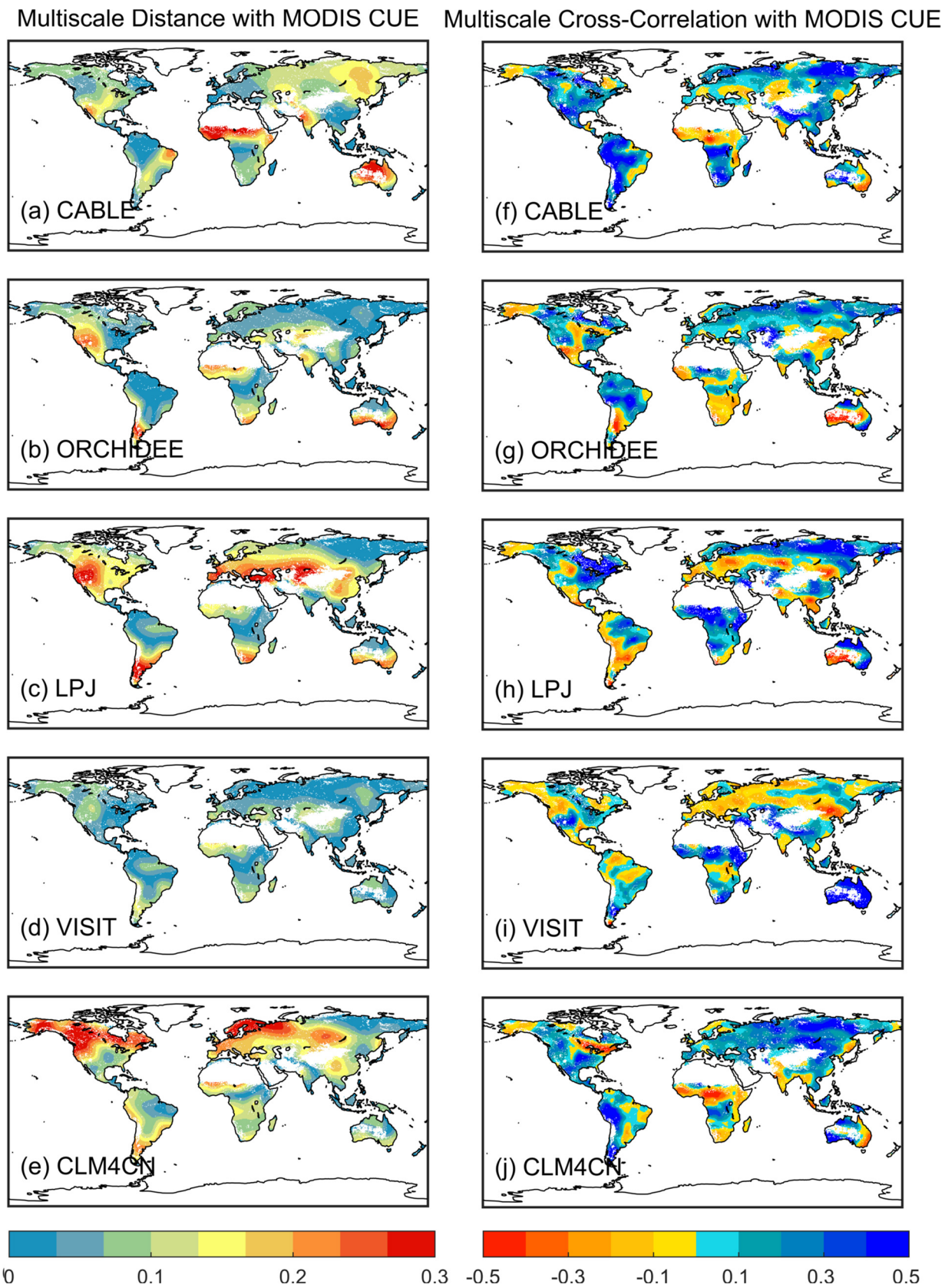


**Fig. 3.** Comparisons between the spatial patterns of carbon use efficiency (CUE) from MODIS satellite data and from five process-based models based on (a)-(e) absolute distance analysis and (f)-(j) cross-correlation analysis from the comparison map profile method.

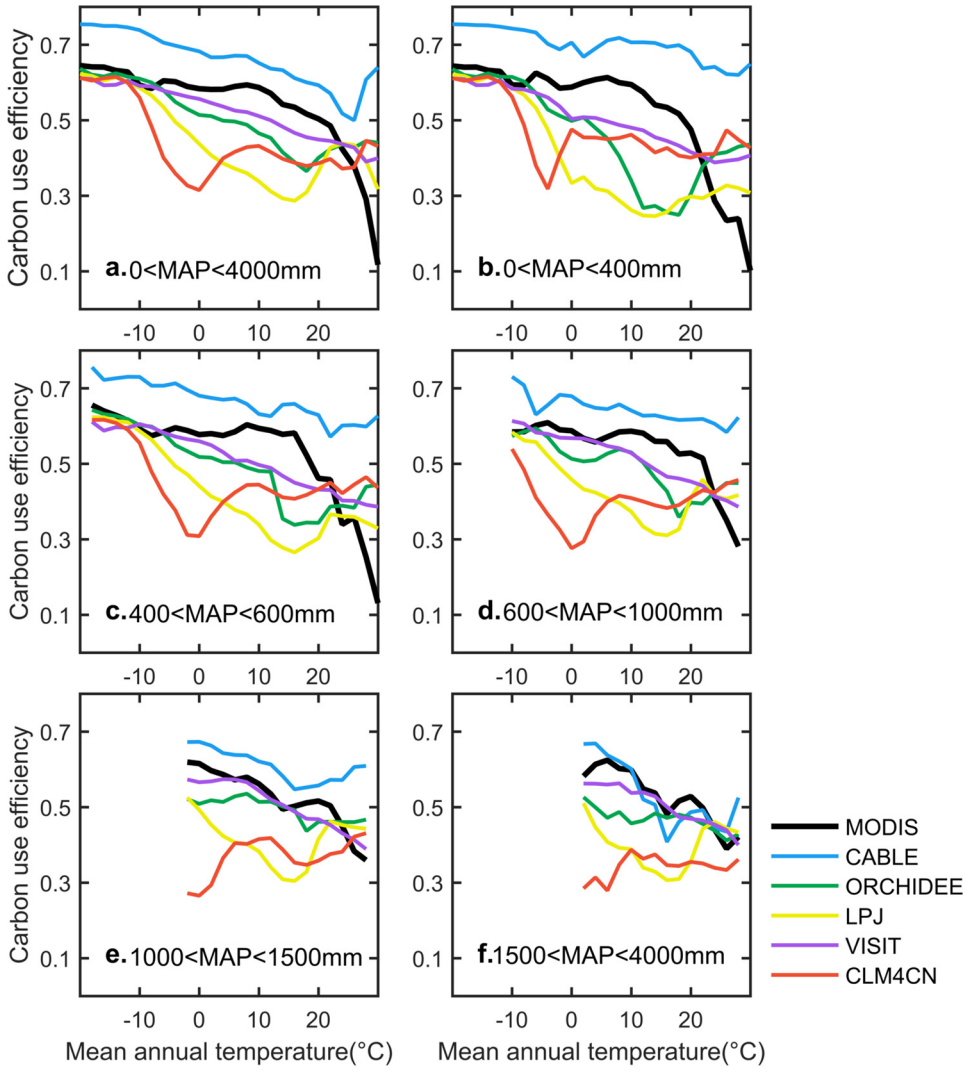


**Fig. 4.** The responses of vegetation carbon use efficiency (CUE) to mean annual temperature (MAT) for different precipitation bins.

models, except that of LPJ, are consistent with that from MODIS data. In LPJ, CUE values are almost constant with increasing precipitation. However, when we further divided the continuum of MAT into different ranges to separate the combined effects of temperature and precipitation, as shown in Fig. 5b–f, generally there is no apparent change in MODIS CUE with rising MAP under different MAT bins, whereas some of the process-based models show positive or negative trends. For instance, ORCHIDEE CUE shows an obvious increasing trend with rising MAP in the MAT interval between 10 to 20 °C, and CABLE CUE decreases with enhanced MAP when MAT is higher than 15 °C.

In order to assess the potential effect of shortwave radiation on CUE, we also performed partial correlation between CUE and radiation after statistically controlling effects of temperature and precipitation. We found that the partial correlation pattern of CUE to radiation is not so obvious (Fig. A.6 in Supplementary materials). In addition, the CUE – MAT and CUE – MAP relationships diagnosed in Figs. 4 and 5 are confirmed by results of partial correlation analysis between CUE and MAT/MAP (Figs. A.4 and 5 in Supplementary materials). Further, temperature and precipitation always outweigh radiation in driving the spatial variation of CUE, and MAT is the distinct dominant effect in each dataset (Fig. A.7 in Supplementary materials).

## 4. Discussion

### 4.1. The main differences in the spatial patterns of CUE among different datasets

Two processes — photosynthesis and autotrophic respiration — are fundamental determinants of vegetation CUE. We have summarized the main processes and parameters in the simulation of leaf photosynthesis and autotrophic respiration for each of process-based models and MODIS product (Table A.2 in Supplementary materials). The parameterization of these two processes varies among different datasets, which could constitute a major source of data spread in the estimation of CUE. However, sources of uncertainties exist for the estimations of both these two processes, which reduce their explanatory powers (Atkin et al., 2008; Anav et al., 2015). Further, the uncertainties in photosynthesis (GPP here) and respiration ($R_a$ here) estimation may not be the same. For instance, we find that the percentage differences of $R_a$ among different products are consistently higher than the corresponding percentage differences of GPP (Fig. A.8 in Supplementary materials). Therefore, the differences in CUE between MODIS data and that from the five process-based models shall be mainly attributed to their differences in $R_a$. The finding of the dominant role of $R_a$ in controlling CUE difference among various models is further confirmed by results of partial correlation analysis between the three components of Eq. (7) (Fig. A.9 in Supplementary materials).

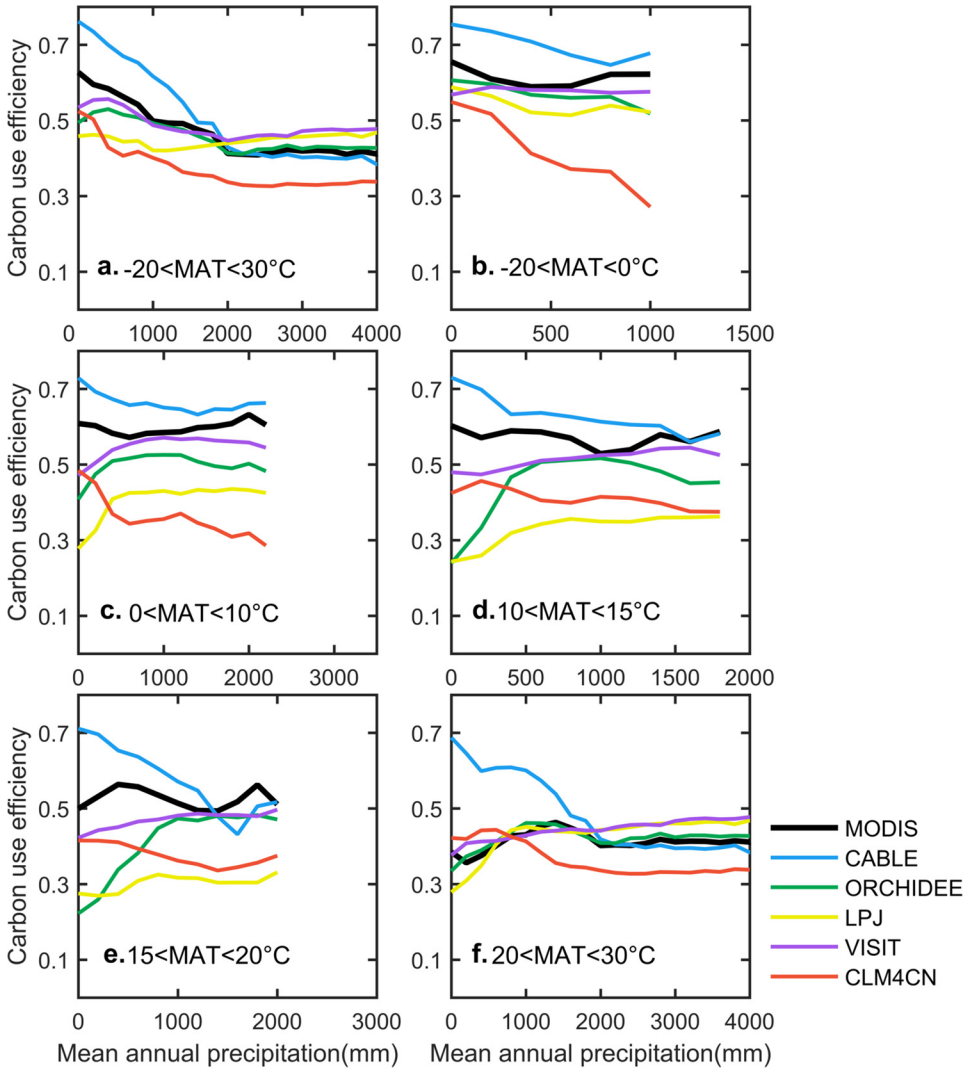


**Fig. 5.** The responses of vegetation carbon use efficiency (CUE) to mean annual precipitation (MAP) for different temperature bins.

Our understanding of $R_a$ is currently very limited (Atkin et al., 2008; Piao et al., 2010). Both in MODIS satellite data and most process-based models, $R_a$ consists of two parts: maintenance respiration ($R_m$) and growth respiration ($R_g$). $R_m$ is usually calculated as a function of temperature and living biomass (Piao et al., 2010); and $R_g$ is often assumed as a constant proportion of vegetation productivity (Pan et al., 2014; Running & Zhao, 2015). The model parameterization in the estimation of $R_m$ and $R_g$ (and consequently $R_a$) spans a diverse range across different datasets, potentially resulting in strikingly different $R_a$ outputs. For instance, in CLM4CN, the $R_g$ is calculated as 30% of the total assimilated carbon, and in LPJ $R_g$ is estimated to be 25% of the difference between GPP and $R_m$. In contrast, MODIS $R_g$ is prescribed to be 25% of NPP (Table A.2 in Supplementary materials).

Furthermore, in addition to different estimations in $R_a$, both MODIS satellite data and the five process-based models also show some differences in their GPP outputs (Fig. A.8 in Supplementary materials). MODIS generally produces a lower GPP than that from process-based models, which is partly attributed to the possibility that the remotely sensed FPAR used in the MODIS algorithm includes the impact of human disturbance on vegetation growth. By contrast, the process-based models generally simulate the potential LAI, which is a hypothetic condition without considering extensive human interference (Anav et al., 2015). But the process-based models still diverge in modelled GPP because of different structures and parameters. For example, in CABLE and VISIT, GPP is estimated based upon the two-leaf canopy model (Wang & Leuning, 1998) and dry-matter production theory (Monsi and Saeki, 1953), but other models adopt Farquhar photosynthesis module in photosynthesis (Table A.2 in Supplementary materials).

Two of the process-based models, CABLE and CLM4CN, include explicit modes of nitrogen availability, which allows the regulation of potential $CO_2$ fertilization effect by nitrogen limitation (Vitousek & Howarth, 1991). The two models produce lower GPP than the other three models (Fig. A.8 in Supplementary materials), but still higher than MODIS GPP. On the other hand, considering the fact that nitrogen limitation not just constrains the productivity of living biomass (Zhang et al., 2013), but also affects $R_a$, the final impact of nitrogen limitation on ecosystem CUE, thus far, is still unclear. In fact, the models with nitrogen modes, CABLE and CLM4CN, produce distinctly different CUE values with no evident regularity compared with results from the other three models (Fig. 2 and Table A.3 in Supplementary materials). Further research, especially those model inter-comparisons with different nitrogen supplies, is needed to further illuminate the effect of nitrogen cycle and nitrogen limitation on ecosystem CUE.

Another cause of the discrepancies in vegetation CUE estimations may come from the inconsistency in the land-cover maps used by the different models and the satellite product. For example, VISIT defines 16 plant function types (PFTs; Ito, 2010), while ORCHIDEE and CABLE use 12 and 10 PFTs, respectively (Krinner et al., 2005; Lu et al., 2013). These different PFT selections can result in discrepancies in both GPP

and $R_a$ simulations, because predefined ecological functions of PFTs vary among different models (Poulter et al., 2011; Li et al., 2016).

### 4.2. Responses of CUE to climatic variables

Both MODIS satellite data and process-based models produce spatially varied CUE, and the examination of the CUE spatial patterns may lead to a better understanding of the climate control of CUE. Here, we focus our discussions on the spatial pattern of CUE in response to changes in MAT and MAP.

The global variation of temperature affects both the photosynthesis and autotrophic respiration rates, resulting in the change of vegetation CUE (Giardina et al., 2003). Previous research has suggested that $R_a$ increases exponentially with MAT (Ryan et al., 1995; Piao et al., 2010), while photosynthetic rates increase to a temperature optimum and decline afterwards (Berry & Bjorkman, 1980). Hence, $R_a$ is more sensitive to MAT than GPP, especially in the high-temperature end (Fig. 4). In colder regions, vegetation requires relatively less energy to maintain living tissues, resulting in the relatively lower respiratory costs and higher CUE (Ryan et al., 1994). On the other hand, vegetation growth is constrained by a short growing-season length. Rising temperature could extend the growing season length and significantly increase GPP (Piao et al., 2007, 2010). Consequently, in cold regions the temperature-sensitivity of CUE is lower because the temperature-sensitivities of GPP and $R_a$ are of comparable size. In warm regions, especially in the tropics where the growing season is long, by contrast, respiratory costs are higher, leading to a lower CUE (Zhang et al., 2009). Furthermore, temperature sensitivity of CUE also changes among different products. For instance, compared with results from the five process-based models, MODIS CUE tends to decline more sharply in response to increasing temperature, especially in warm and dry conditions (Fig. 4). This is probably because the parameter used to calculate the temperature sensitivity of $R_a$ in MODIS is relatively higher (Ise et al., 2010).

The general decline of vegetation CUE to MAP change at the global scale shown in Fig. 5a is consistent with the results found in previous studies (Chambers et al., 2004; Zhang et al., 2009; Kwon & Larsen, 2013). Several theories, including shortage of soil oxygen, increase in cloudiness, and reduced organic matter decomposition rate, have been proposed to explain this trend of CUE decreasing as MAP increases (Schuur & Matson, 2001; Zhang et al., 2009). Here we argue that the higher value of CUE in relatively cold and dry areas may also be responsible for the negative trend of CUE with rising MAT. In other words, the apparent response of CUE to precipitation is confounded by the positive correlation between temperature and precipitation. When MAT is kept nearly constant to remove the effect of co-variations between MAT and MAP, vegetation CUE in all the datasets show no trends to MAP changes, with few exceptions. These findings indicate that the spatial variation of CUE is mainly controlled by MAT rather than MAP, implying a positive feedback between climate warming and vegetation CUE.

## 5. Conclusions

In summary, our results show considerable differences in CUE among different approaches, particularly in the temperate regions. Reducing these uncertainties should be given a high priority through validating current process-oriented carbon models with observation data. Unfortunately, in situ data that can be used for characterizing the global patterns of CUE with sufficient accuracy are still very scarce due to vegetation heterogeneity and insufficient sampling. Furthermore, given the primary role of systematic between-approach differences in $R_a$ in causing the large discrepancy in CUE estimations, understanding mechanisms behind spatio-temporal change in $R_a$ is a critical step towards better quantifying global CUE and improving future projections of carbon cycle dynamics.

## Acknowledgements

This study was supported by the National Key R&D Program of China (2017YFA0604702), the National Natural Science Foundation of China (41530528 and 31621091), and National Youth Top-notch Talent Support Program in China. Funding for this study was also provided by undergraduate student research training program of the Ministry of Education. A.P. C. acknowledges the support of a research fellowship provided by the Purdue University Department of Forestry and Natural Resources.

## Appendix A. Supplementary data

Supplementary material related to this article can be found, in the online version, at doi:https://doi.org/10.1016/j.agrformet.2018.03.009.

## References

Amthor, J.S., 2000. The McCree-de wit-penning de vries-thornley respiration paradigms: 30 years later. Ann. Bot. 86, 1–20.
Anav, A., Friedlingstein, P., Beer, C., et al., 2015. Spatiotemporal patterns of terrestrial gross primary production: a review. Rev. Geophys. 53, 785–818.
Atkin, O.K., Atkinson, L.J., Fisher, R.A., et al., 2008. Using temperature-dependent changes in leaf scaling relationships to quantitatively account for thermal acclimation of respiration in a coupled global climate-vegetation model. Glob. Change Biol. 1 (4), 2709–2726.
Berry, J., Bjorkman, O., 1980. Photosynthetic response and adaptation to temperature in higher plants. Annu. Rev. Plant Physiol. 31, 491–543.
Bloom, A.A., Exbrayat, J.F., van der Velde, I.R., et al., 2016. The decadal state of the terrestrial carbon cycle: global retrievals of terrestrial carbon allocation, pools, and residence times. Proc. Natl. Acad. Sci. 1 (13), 1285–1290.
Bradford, M.A., Crowther, T.W., 2013. Carbon use efficiency and storage in terrestrial ecosystems. New Phytol. 199, 7–9.
Campioli, M., Vicca, S., Luyssaert, S., et al., 2015. Biomass production effciency controlled by management in temperate and boreal ecosystems. Nat. Genet. 8, 843–846.
Chambers, J.Q., Tribuzy, E.S., Toledo, L.C., et al., 2004. Respiration from a tropical forest ecosystem: partitioning of sources and low carbon use efficiency. Ecol. Appl. 14, S72–S88.
Chapin, F.S., Matson, P.A., Mooney, H.A., Chapin, M.C., 2002. Principles of Terrestrial Ecosystem Ecology. Springer-Verlag, New York, NY.
De Lucia, E.H., Drake, J.E., Thomas, R.B., Gonzalez-Meler, M., 2007. Forest carbon use efficiency: is respiration a constant fraction of gross primary production? Glob. Change Biol. 13, 1157–1167.
Gaucherel, C., Alleaume, S., Hély, C., 2008. The comparison map profile method: a strategy for multiscale comparison of quantitative and qualitative images. IEEE Trans. Geosci. Remote Sens. 46, 2708–2719.
Giardina, C.P., Ryan, M.G., Binkley, D., Fownes, J.H., 2003. Primary production and carbon allocation in relation to nutrient supply in a tropical experimental forest. Glob. Change Biol. 9, 1438–1450.
Gifford, R.M., 2003. Plant respiration in productivity models: conceptualisation, representation and issues for global terrestrial carbon-cycle research. Funct. Plant Biol. 30, 171–186.
Grömping, U., 2006. Relative importance for linear regression in R: the package relaimpo. J. Stat. Softw. 1 (7), 1–27.
Harris, I., Jones, P.D., Osborn, T.J., Lister, D.H., 2014. Updated high-resolution grids of monthly climatic observations—the CRU TS3. 10 Dataset. Int. J. Climatol. 34, 623–642.
Huang, M.T., Piao, S.L., Sun, Y., et al., 2015. Change in terrestrial ecosystem water-use efficiency over the last three decades. Glob. Change Biol. 21, 2366–2378.
Huntingford, C., Cox, P.M., Mercado, L.M., et al., 2011. Highly contrasting effects of different climate forcing agents on terrestrial ecosystem services. Philos. Trans. A: Math Phys. Eng. Sci. (369), 2026–2037.
Ise, T., Litton, C.M., Giardina, C.P., Ito, A., 2010. Comparison of modeling approaches for carbon partitioning: impact on estimates of global net primary production and equilibrium biomass of woody vegetation from MODIS GPP. J. Geophys. Res. Biogeosci. 115 (G04025). http://dx.doi.org/10.1029/2010JG001326.
Ito, A., 2010. Changing ecophysiological processes and carbon budget in East Asian ecosystems under near-future changes in climate: implications for long-term monitoring from a process-based model. J. Plant Res. 1 (23), 577–588.
Lindeman, R.H., Merenda, P.F., Gold, R.Z., 1980. Introduction to Bivariate and Multivariate Analysis. Foresman, Glenview IL.
Krinner, G., Viovy, N., de Noblet-Ducoudré, N., et al., 2005. A dynamic global vegetation model for studies of the coupled atmosphere-biosphere system. Glob. Biogeochem. Cycles 1 (9), 1–33.
Kwon, Y., Larsen, C.P.S., 2013. Effects of forest type and environmental factors on forest carbon use efficiency assessed using MODIS and FIA data across the eastern USA. Int. J. Remote Sens 34, 8425–8448.
Law, B.E., Turner, D., Campbell, J., et al., 2004. Disturbance and climate effects on carbon stocks and fluxes across western Oregon USA. Glob. Change Biol. 10, 1429–1444.

Li, X.R., Zhu, Z.C., Zeng, H., Piao, S.L., 2016. Estimation of gross primary production in China (1982–2010) with multiple ecosystem models. Ecol. Model. 324, 33–44.
Liu, D., Li, Y., Wang, T., et al., 2018. Contrasting responses of grassland water and carbon exchanges to climate change between tibetan plateau and inner Mongolia. Agric. For. Meteorol. 249, 163–175.
Lu, X.J., Wang, Y.P., Ziehn, T., Dai, Y.J., 2013. An efficient method for global parameter sensitivity analysis and its applications to the Australian community land surface model (CABLE). Agric. For. Meteorol. 182, 292–303.
Mäkelä, A., Valentine, H.T., 2001. The ratio of NPP to GPP: evidence of change over the course of stand development. Tree Physiol. 21, 1015–1030.
Metcalfe, D.B., Meir, P., Aragão, L.E.O., et al., 2010. Shifts in plant respiration and carbon use efficiency at a large-scale drought experiment in the eastern amazon. New Phytol. 187, 608–621.
Moorcroft, P.R., 2006. How close are we to a predictive science of the biosphere? Trends Ecol. Evol. 21, 400–407.
Pan, S.F., Tian, H.Q., Dangal, S.R.S., et al., 2014. Modeling and monitoring terrestrial primary production in a changing global environment: toward a multiscale synthesis of observation and simulation. Adv. Meteorol. 2014, 1–17.
Piao, S.L., Friedlingstein, P., Ciais, P., Viovy, N., Demarty, J., 2007. Growing season extension and its impact on terrestrial carbon cycle in the northern hemisphere over the past 2 decades. Glob. Biogeochem. Cycles 21, 49–53.
Piao, S.L., Luyssaert, S., Ciais, P., et al., 2010. Forest annual carbon cost: a global-scale analysis of autotrophic respiration. Ecology 91, 652–661.
Piao, S.L., Nan, H.J., Huntingford, C., et al., 2014. Evidence for a weakening relationship between interannual temperature variability and northern vegetation activity. Nat. Commun. 5, 1–7.
Piao, S.L., Yin, G.D., Tan, J.G., et al., 2015. Detection and attribution of vegetation greening trend in China over the last 30 years. Glob. Change Biol. 21, 1601–1609.
Piao, S.L., Liu, Z., Wang, T., et al., 2017. Weakening temperature control on the interannual variations of spring carbon uptake across northern lands. Nat. Clim. Change 7, 359–363.
Potter, C.S., Randerson, J.T., Field, C.B., et al., 1993. Terrestrial ecosystem production: a process model based on global satellite and surface data. Glob. Biogeochem. Cycles 7, 811–841.
Poulter, B., Ciais, P., Hodson, E., et al., 2011. Plant functional type mapping for earth system models. Model Dev. 4, 993–1010.
Prentice, I.C., Liang, X., Medlyn, B.E., Wang, Y.P., 2015. Reliable, robust and realistic: the three r's of next-generation land-surface modelling. Atherosclerosis (Amsterdam Netherlands) 15, 5987–6005.
Running, S.W., Coughlan, J.C., 1988. A general model of forest ecosystem processes for regional applications. I. Hydrologic balance, canopy gas-exchange and primary production processes. Ecol. Model. 42, 125–154.
Running, S.W., Nemani, R.R., Heinsch, F.A., et al., 2004. A continuous satellite-derived measure of global terrestrial primary production. BioScience 54, 547–560.
Running, S.W., Zhao, M.S., 2015. Daily GPP and Annual NPP (MOD17A2/A3) Products NASA Earth Observing System MODIS Land Algorithm. MOD17 User's Guide. 28 pp. .
Ryan, M.G., Linder, S., Vose, J.M., Hubbard, R.H., 1994. Dark respiration of pines. Ecol. Bull. 43, 50–63.
Ryan, M.G., Gower, S.T., Hubbard, R.M., et al., 1995. Woody tissue maintenance respiration of four conifers in contrasting climates. Oecologia 101, 133–140.
Ryan, M.G., Lavigne, M.B., Gower, S.T., 1997. Annual carbon cost of autotrophic respiration in boreal forest ecosystems in relation to species and climate. J. Geophys. Res. 102, 28871–28883.
Schuur, E.A.G., Matson, P.A., 2001. Net primary productivity and nutrient cycling across a mesic to wet precipitation gradient in hawaiian montane forest. Oecologia 128, 431–442.
Sitch, S., Smith, B., Prentice, I.C., et al., 2003. Evaluation of ecosystem dynamics, plant geography and terrestrial carbon cycling in the LPJ dynamic global vegetation model. Glob. Change Biol. 9, 161–185.
Sjöström, M., Zhao, M., Archibald, S., et al., 2013. Evaluation of MODIS gross primary productivity for africa using eddy covariance data. Remote Sens. Environ. 131, 275–286.
Thornton, P.E., Lamarque, J.F., Rosenbloom, N.A., Mahowald, N.M., 2007. Influence of carbon-nitrogen cycle coupling on land model response to $CO_2$ fertilization and climate variability. Glob. Biogeochem. Cycles 21 (GB4018). http://dx.doi.org/10.1029/2006GB002868.
Van Iersel, M.W., 2003. Carbon use efficiency depends on growth respiration, maintenance respiration, and relative growth rate. A case study with lettuce. Plant Cell Environ. 26, 1441–1449.
Vicca, S., Luyssaert, S., Peñuelas, J., et al., 2012. Fertile forests produce biomass more efficiently. Ecol. Lett. 15, 520–526.
Viovy, N., 2015. CRU-NCEP v6.1 Dataset. http://dods.extra.cea.fr/store/p529viov/cruncep/.
Vitousek, P.M., Howarth, R.W., 1991. Nitrogen limitation on land and in the sea: how can it occur? Biogeochemistry 13, 87–115.
Wang, T., Lin, X., Peng, S.S., et al., 2014a. Multimodel projections and uncertainties of net ecosystem production in China over the twenty-first century. Chin. Sci. Bull. 59, 4681–4691.
Wang, T., Lin, X., Liu, Y.W., et al., 2016. Causes of uncertainty in China's net primary production over the 21st century projected by the CMIP5 earth system models. Int. J. Climatol. 36, 2323–2334.
Wang, X.H., Piao, S.L., Ciais, P., et al., 2014b. A two-fold increase of carbon cycle sensitivity to tropical temperature variations. Nature 506, 212–215.
Wang, X.Y., Wang, T., Liu, D., et al., 2017. Moisture-induced greening of the South Asia over the past three decades. Glob. Change Biol. 23, 4995–5005.
Wang, Y.P., Law, R.M., Pak, B., 2010. A global model of carbon, nitrogen and phosphorus cycles for the terrestrial biosphere. Biogeosciences 7, 2261–2282.
Wang, Y.P., Kowalczyk, E., Leuning, R., et al., 2011. Diagnosing errors in a land surface model (CABLE) in the time and frequency domains. J. Geophys. Res. Biogeosci. 116, 1–18.
Wu Ciais, D.H.P., Viovy, N., et al., 2018. Asymmetric responses of primary productivity to altered precipitation simulated by ecosystem models across three long-term grassland sites. Biogeosci. Discuss. http://dx.doi.org/10.5194/bg-2018-53. in review.
Zhang, Q., Pitman, A.J., Wang, Y.P., Dai, Y.J., Lawrence, P.J., 2013. The impact of nitrogen and phosphorous limitation on the estimated terrestrial carbon balance and warming of land use change over the last 156 yr. Earth Syst. Dyn. 4, 333–345.
Zhang, Y.J., Xu, M., Chen, H., Adams, J., 2009. Global pattern of NPP to GPP ratio derived from MODIS data: effects of ecosystem type, geographical location and climate. Glob. Ecol. Biogeogr. 18, 280–290.
Zhang, Y.J., Yu, G.R., Yang, J., et al., 2014. Climate-driven global changes in carbon use efficiency. Glob. Ecol. Biogeogr. 23, 144–155.
Zhao, M.S., Running, S.W., Nemani, R.R., 2006. Sensitivity of moderate Resolution imaging spectroradiometer (MODIS) terrestrial primary production to the accuracy of meteorological reanalyses. J. Geophys. Res. Biogeosci. 111 (G01002). http://dx.doi.org/10.1029/2004JG000004.
Zhao, M.S., Running, S.W., 2010. Drought-induced reduction in global terrestrial net primary production from 2000 through 2009. Science 329, 940–943.
Zhu, Z.C., Piao, S.L., Myneni, R.B., et al., 2016. Greening of the earth and its drivers. Nat. Clim. Change 6, 791–795.